Chem. Pap. (2018) 72:903–919
https://doi.org/10.1007/s11696-017-0333-2

ORIGINAL PAPER

Synthesis, spectroscopic characterization, X-ray structure, DFT calculations, and antimicrobial studies of diorganotin (IV) complexes of monotopic oxygen nitrogen donor Schiff base

Shaukat Shujah[1] · Saqib Ali[2] · Nasir Khalid[3] · Mohammad Jane Alam[4] · Shabbir Ahmad[4] · Auke Meetsma[5]

Received: 3 June 2017 / Accepted: 31 October 2017 / Published online: 7 November 2017

Abstract Seven new diorganotin(IV) complexes, [Me_2SnL] (**1**), [Et_2SnL] (**2**), [(*n*-Bu_2SnL] (**3**), [Ph_2SnL] (**4**), [(*n*-Oct_2SnL] (**5**), [tert-Bu_2SnL] (**6**), and [*n*-BuClSnL] (**7**) have been synthesized from the reaction of *N*′-(2-hydroybenzylidene)-4-tert-butylbenzohydrazide (H_2L) with the corresponding diorganotin(IV) dichloride/oxide or organotin(IV) chloride dihydroxide. The synthesized compounds were structurally characterized by FT-IR, multinuclear NMR (^{1}H and ^{13}C) spectroscopies, elemental analysis, mass spectrometry, DFT/(B3LYP) calculations, and, for ligand single crystal, X-ray diffraction analysis. Spectroscopic evidence affirms coordination of ligand to the dialkyltin(IV) moieties through oxygen nitrogen donor sites in iminol form. The $^1J(^{119}Sn, ^{13}C)$ coupling constants, 584-655 Hz and $^2J(^{119}Sn\text{-}^1H)$ coupling constant, 79 Hz for complex (**1**), suggest pentacoordination around Sn atom in solution. Single-crystal X-ray structure of ligand show its existence in amido form. Supramolecular architecture mediated by N(2)-H···O(2) and C-H…π interactions is formed in solid state. The DFT calculations have been performed to obtain various structure-based molecular properties as well as to support experimental results. The synthesized compounds were screened in vitro against various human pathogenic microbial strains. *Escherichia coli* and *Staphylococcus aureus* were most visibly inhibited by complexes (**4**) and (**7**). Highest antifungal activity was shown by compound (**6**) against *Fusarium solani*. Compound (**3**) displayed highest cytotoxicity among synthesized compounds with LD_{50} 0.44µg/mL.

Electronic supplementary material The online version of this article (https://doi.org/10.1007/s11696-017-0333-2) contains supplementary material, which is available to authorized users.

✉ Shaukat Shujah
shaukat.shujah@yahoo.com

[1] Department of Chemistry, Kohat University of Science and Technology, Kohat 26000, Pakistan

[2] Department of Chemistry, Quaid-i-Azam University, Islamabad 45320, Pakistan

[3] Chemistry Division, Pakistan Institute of Nuclear Science and Technology, PO Nilore, Islamabad, Pakistan

[4] Department of Physics, Aligarh Muslim University, Aligarh, India

[5] Chemical Physics, Crystal Structure Center, Zernike Institute for Advanced Materials, University of Groningen, Nijenborgh 4, 9747 AG Groningen, The Netherlands

Graphical Abstract

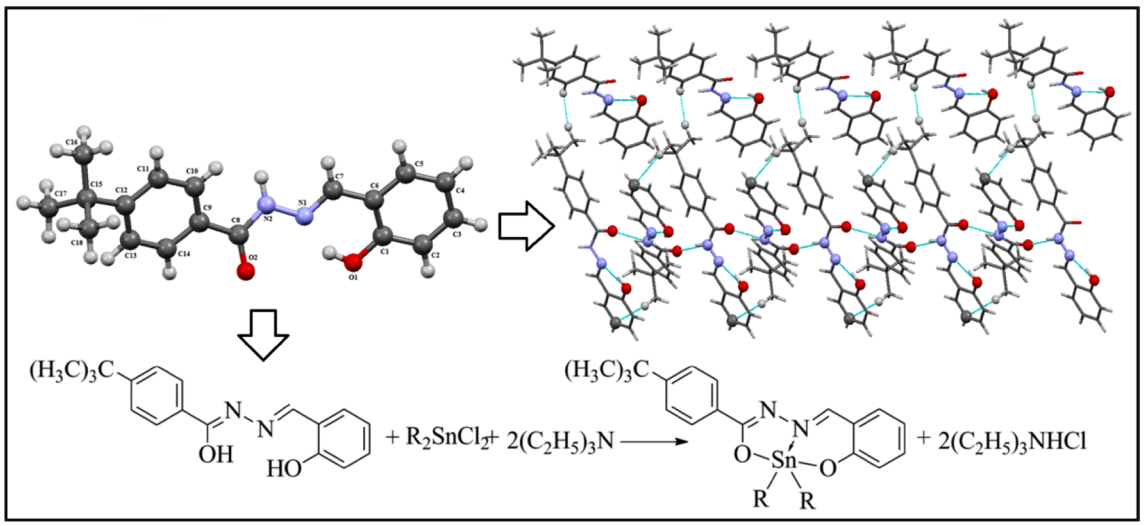

Keywords Diorganotin(IV) complexes · DFT calculations · Antibacterial activity · Antifungal · Activity · Cytotoxicity

Introduction

Organotin(IV) compounds have been the center of attention of many research groups primarily due to diversity in their structures and wide range of applications. Substantial interest has been shown in their biological and pharmaceutical activities as anti-diabetic (Roy et al. 2016), antitumor (Fani et al. 2015), antituberculosis (Kovala-Demertzi et al. 2009), antileishmanial (Sirajuddin et al. 2014), and antimicrobial agents (Sharma et al. 2016). The biochemical behavior of these complexes is primarily influenced by the oxidation state, coordination number of metal atom, geometry, and thermodynamic and kinetic characteristics of complex. Furthermore, the groups directly bonded with tin atom not only confer special pharmaceutical characteristics to these compounds (Girasolo et al. 2014) by modifying their fat solubility but also play an essential role in the transportation of these compounds to specific sites (Gholivand et al. 2016).

Antimicrobial agents act on vital microbial functions like cell wall synthesis, nucleic acid synthesis, and folate metabolism, and may impede the role of cell membrane and ribosome. However, the microbes have developed ways of not being affected by these compounds. The emergence of such bacterial and fungal multidrug-resistant strains has increased the need to design and synthesize compounds which can be effectively used against such pathogens (Zhang et al. 2016).

Density functional theory (DFT) calculations of chemical species have become an integral part of research, where they play an important role in supplementing and supporting interpretation of experimental data. Such calculations well reproduce the experimental results and also provide various structure-based molecular properties. The B3LYP (Becke, 3-parameter, Lee–Yang–Parr) hybrid functional in DFT has been very popular, because it shows trade-off between accuracy and computational cost than the post Hartree–Fock methods and generally yields comparable results.

In continuation with our previous studies on diorganotin(IV) complexes and the rising demand for an efficient metal based compound that can inhibit the growth of pathogens, we report herein the synthesis of N′-(2-hydroxybenzylidene)-4-tert-butylbenzohydrazide (**H_2L**) and seven new diorganotin(IV) derivatives [R_2SnL] (R=–CH_3 (**1**), –C_2H_5 (**2**), *n*-C_4H_9 (**3**), –C_6H_5 (**4**), –C_8H_{17} (**5**), *-tert*-C_4H_9 (**6**), *n*-C_4H_9Cl (**7**) L=N′-(2-oxydobenzylidene)-4-tert-butylbenzohydrazide. All the compounds were characterized by FT-IR, multinuclear NMR (^{1}H and ^{13}C), elemental analysis, mass spectroscopy, DFT/B3LYP calculations, and screened against selected pathogenic bacterial and fungal strains. Cytotoxicity assessed by in vivo lethality to brine shrimp nauplii is also reported.

Experimental

Materials and methods

Salicyldehyde, 4-tert-butylbenzoic hydrazide, triethylamine, dimethyltin(IV) dichloride, diethyltin(IV) dichloride, dibutyltin(IV) dichloride, diphenyltin(IV) dichloride, dioctyltin(IV) oxide, and butyltin(IV) chloridedihydroxide were purchased from Sigma-Aldrich and used as received.

Solvents used for synthesis were purified by standard procedures (Armarego and Chai 2013).

Elemental analyses (C, H, and N) were performed using a Leco CHNS 932 analyzer. The infrared (IR) spectra (4000–400 cm^{-1}) were recorded with a Bio-Rad Excaliber FT-IR, model FTS 300 MX spectrophotometer (USA). Multinuclear NMR (^1H and ^{13}C) spectra were recorded on a Bruker ARX 300 MHz-FT-NMR Switzerland using TMS as internal reference. Chemical shifts (δ) and coupling constants (*J*) are provided in ppm and Hz, respectively. The mass spectral measurements were made on an MAT-311A Finnigan (Germany). The X-ray diffraction study was conducted on Bruker SMART APEX CCD diffractometer. Data integration and global cell refinement were accomplished with program SAINT and program suite SAINTPLUS used for space group determination (XPREP). The structure was solved by Patterson method; extension of model was accomplished by direct method and applied to different structure factors using program DIRDIF. All refinement-related calculations and graphics were made with PLUTO and PLATON package (Beurskens et al. 1999; Bruker 2006; Meetsma 2001; Sheldrick 1997; Spek 1998).

Synthesis of ligand

Salicylaldehyde 0.64 g (5.20 mmol) and 4-tert-butylbenzoic hydrazide 1.0 g (5.20 mmol) were reacted in ethanol (50 mL). The reaction mixture was constantly stirred and refluxed for 2 h. On cooling, the solution afforded a yellowish white crystalline product (Scheme 1).

*N′-(2-hydroxybenzylidene)-4-tert-butylbenzohydrazide(**H$_2$L**)*

Yield, 1.3 g, 85%; m.p. 194–196 °C; elemental analysis (%), calcd. for $C_{18}H_{20}N_2O_2$: C, 72.95; H, 6.80; N, 9.45. Found: C, 72.91; H, 6.78; N, 9.48. FT-IR (KBr) υ_{max}/cm^{-1}: 1686 (s, C=O), 3180 (s, NH), 1616 (m, C=N), 3410 (s, OH). EI-MS m/z (%): $[M]^+$ 296(7.1), [M-*tert*-ButPh]$^+$ 163(4.1), [tert-BuPhCO]$^+$ 161(100.0), $[Ph]^+$ 77(14.7), $[But]^+$ 57(14.9). ^1H NMR (DMSO-*d6*, ppm): 6.95 (d, 1H, PhC2-H, $J = 9.0$ Hz), 7.30 (t, 1H, PhC3-H, $J = 8.4$ Hz), 6.92 (t, 1H, PhC4-H, $J = 8.4$ Hz), 7.22 (d, 1H, PhC5-H, $J = 7.8$ Hz), 8.64 (s, 1H, CH=N), 7.89 (d, 2H, PhC10,10′-H, $J = 8.4$ Hz), 7.56 (d, 2H, PhC11,11′-H, $J = 8.1$ Hz), 1.32 (s, 9H, $C(CH_3)_3$). ^{13}C NMR (DMSO-*d6*, ppm): 158.0, 131.8, 130.0, 119.8, 119.1, 116.9 (PhC1-C6), 148.6 (HC=N), 163.2 (OCNN), 155.4, 130.5, 128.0, 125.8 (PhC9-C12), 35.2, 31.4 ($C(CH_3)_3$).

Synthesis of the diorganotin(IV) complexes (1-7)

Two separate methods were employed for the synthesis of diorganotin(IV) derivatives.

Method I: *N′*-(2-hydroxybenzylidene)-4-tert-butylbenzohydrazide 3.0 mmol (0.89 g) and triethylamine 6 mmol (0.83 mL) were mixed and stirred in toluene (100 mL) for 15 min. Dialkyltin dichloride 3.0 mmol (dimethyl, diethyl, dibutyl, diphenyl, and ditertbutyl) was then added and solution further stirred for 4 h. The Et_3NHCl salt formed within the yellow solution was filtered off and filtrate rotary evaporated under reduced pressure to get a yellow product (Scheme 2).

Method II: Dioctyltin(IV) and butylchlorotin(IV) derivatives were synthesized by refluxing dioctyltin(IV) oxide or butyltin(IV) chloridedihydroxide and *N′*-(2-hydroxybenzylidene)-4-tert-butylbenzohydrazide in toluene (100 mL) for 3 h. The water formed during the reaction was removed by the Dean–Stark apparatus. Removal of solvent by evaporation under reduce pressure afforded the product (Scheme 2). All the complexes were recrystallized from chloroform *n*-hexane (4:1) mixture; however, no suitable crystal for X-ray diffraction study was obtained. The structure and numbering template of diorganotin(IV) derivatives is also illustrated in Scheme 2.

*Dimethyltin(IV) [N′-(2-oxidobenzylidene)-N-(oxido-(4-tert-butylphenyl)methylene)hydrazine] (**1**)*

Yield: 1.1 g, 84%; m.p. 118–120 °C; elemental analysis (%), calcd. for $C_{20}H_{24}N_2O_2Sn$: C, 54.21; H, 5.46; N, 6.32. Found: C, 54.25; H, 5.49; N, 6.29. FT-IR (KBr) υ_{max}/cm^{-1}: 1608 (m, C=N), 1070 (w, N–N), 562 (w, Sn–O), 461 (w, Sn–N). EI-MS, m/z (%): $[M]^+$ 444(50.1); $[M–Me]^+$ 429(9.1); $[M\text{-}2Me]^+$ 414(45.0); $[SnMe]^+$ 135 (28.7); [tert-BuPhCO]$^+$ 161(100.0); $[Sn]^+$ 120(9.4) ^1H NMR ($CDCl_3$ ppm): 6.80 (d, 1H, PhC2-H, $^3J_{H\text{-}H} = 7.8$ Hz), 7.35 (t, 1H, PhC3-H, $^3J_{H\text{-}H} = 8.0$ Hz), 6.76 (t, 1H, PhC4-H, $^3J_{H\text{-}H} = 7.2$ Hz), 7.20 (d, 1H, PhC5-H, $^3J_{H\text{-}H} = 7.8$ Hz), 8.78 (s, 1H, CH = N,

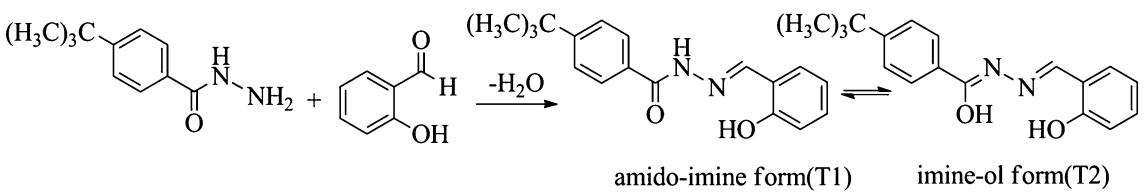

Scheme 1 Synthesis of N-(2-hydroxybenzylidene)-4-tert-butylbenzohydrazide (H_2L)

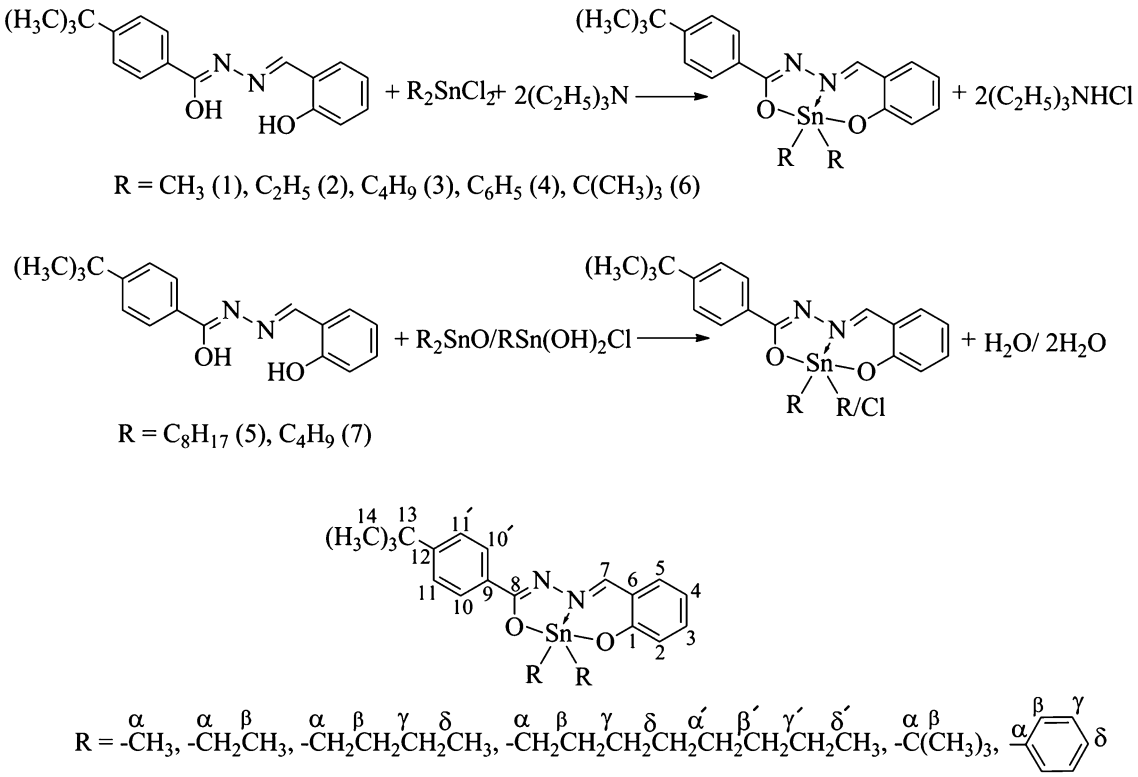

Scheme 2 Synthesis of diorganotin(IV) complexes (1–7) and numbering scheme of alkyl groups bonded to tin atom

^{3}J (^{119}Sn-^{1}H) = 46 Hz), 8.02 (d, 2H, PhC10,10′-H, $^{3}J_{H\text{-}H}$ = 8.4 Hz),7.46 (d, 2H, PhC11,11′-H, $^{3}J_{H\text{-}H}$ = 8.4 Hz), 1.37 (s, 9H, C(CH$_3$)$_3$), 0.85 (s, 6H, SnMe, ^{2}J($^{119/117}$Sn-^{1}H) = 79, 76 Hz). ^{13}C NMR (CDCl$_3$ ppm): 166.3, 135.1, 134.1, 121.7, 117.2, 116.8 (PhC1-C6), 161.1 (HC=N), 169.3 (OCNN), 154.6, 130.4, 127.4, 125.2 (PhC9-C12), 34.9, 31.2 (C(CH$_3$)$_3$), 1.4 (SnMe-C, ^{1}J[$^{119/117}$Sn-^{13}C] = 655 Hz).

*Diethyltin(IV) [N′-(2-oxidobenzylidene)-N-(oxido-(4-tert-butylphenyl)methylene) hydrazine] (**2**)*

Yield: 1.2 g, 88%; m.p. paste; elemental analysis (%), calcd. for $C_{22}H_{28}N_2O_2Sn$: C, 56.08; H, 5.99; N, 5.95. Found: C, 56.11; H, 6.03; N, 5.93. FT-IR (KBr) υ_{max}/cm^{-1}: 1606 (m, C=N), 1077 (w, N–N), 569 (w, Sn–O), 458 (w, Sn–N). EI-MS, m/z (%): [M]$^+$ 472(25.7); [M-Et]$^+$ 443(20.7); [M-2Et]$^+$ 414(44.0); [SnEt]$^+$ 149(2.7); [tert-BuPhCO]$^+$ 161(100.0); [Sn]$^+$ 120(4.6). ^{1}H NMR (CDCl$_3$ ppm): 6.81 (d, 1H, PhC2-H, $^{3}J_{H\text{-}H}$ = 8.4 Hz), 7.34 (t, 1H, PhC3-H, $^{3}J_{H\text{-}H}$ = 7.8 Hz), 6.73 (t, 1H, PhC4-H, $^{3}J_{H\text{-}H}$ = 7.4 Hz), 7.18 (d, 1H, PhC5-H, $^{3}J_{H\text{-}H}$ = 7.8 Hz), 8.79 (s, 1H, CH = N, ^{3}J(^{119}Sn-^{1}H) = 43 Hz), 8.03 (d, 2H, PhC10,10′-H, ^{3}J = 8.4 Hz), 7.46 (d, 2H, PhC11,11′-H, $^{3}J_{H\text{-}H}$ = 8.7 Hz), 1.36 (s, 9H, C(CH$_3$)$_3$), 1. 40-1.51 (m, 4H, SnEtCα-H), 1.32 (t, 6H, SnEtCβ-H, $^{3}J_{H\text{-}H}$ = 7.2 Hz) ^{13}C NMR (CDCl$_3$ ppm): 167.1, 135.0, 134.1, 121.6, 116.9, 116.8 (PhC1-C6), 161.2 (HC = N), 169.7 (OCNN), 154.5, 130.5, 127.4, 125.2 (PhC9-C12), 34.9, 31.2 (C(CH$_3$)$_3$), 14.3 (SnEt-Cα, ^{1}J[$^{119/117}$Sn-^{13}C] = 618 Hz), 9.3 (SnEt-Cβ, ^{2}J[^{119}Sn-^{13}C] = 43 Hz).

*Di-n-butyltin(IV) [N′-(2-oxidobenzylidene)-N-(oxido-(4-tert-butylphenyl)methylene)hydrazine] (**3**)*

Yield: 1.2 g, 78%; m.p. 72–75 °C; elemental analysis (%), calcd. for $C_{26}H_{36}N_2O_2Sn$: C, 59.22; H, 6.88; N, 5.31. Found: C, 59.26; H, 6.84; N, 5.35. FT-IR (KBr) υ_{max}/cm^{-1}: 1610 (m, C = N), 1082 (w, N–N), 570 (w, Sn–O), 465 (w, Sn–N). EI-MS, m/z (%): [M]$^+$ 528(29.7); [M–*n*-Bu]$^+$ 471 (20.1); [M-2*n*-Bu]$^+$ 414(31.6); [Sn(Bu)$_2$]$^+$ 234(6.0); [tert-BuPhCO]$^+$ 161(100.0); [Sn]$^+$ 120(7.5). ^{1}H NMR (CDCl$_3$ ppm): 6.80 (d, 1H, PhC2-H, $^{3}J_{H\text{-}H}$ = 8.4 Hz), 7.34 (t, 1H, PhC3-H, $^{3}J_{H\text{-}H}$ = 7.8 Hz), 6.74 (t, 1H, PhC4-H, $^{3}J_{H\text{-}H}$ = 7.5 Hz), 7.19 (d, 1H, PhC5-H, $^{3}J_{H\text{-}H}$ = 7.8 Hz), 8.78 (s, 1H, CH = N, ^{3}J(^{119}Sn-^{1}H) = 43 Hz), 8.05 (d, 2H, PhC10,10′-H, $^{3}J_{H\text{-}H}$ = 8.7 Hz), 7.48 (d, 2H, PhC11,11′-H, *J* = 8.4), 1.38 (s, 9H, C(CH$_3$)$_3$), 1.64–1.72 (m, 4H, SnBuCα-H), 1.52-1.59 (m, 4H, SnBuCβ-H), 1.35–1.42 (m, 4H, SnBuCγ-H), 0.90 (t, 6H, SnBuCδ-H, $^{3}J_{H\text{-}H}$ = 7.2 Hz) ^{13}C NMR (CDCl$_3$ ppm): 166.9, 134.9, 134.1, 121.6, 117.1, 116.8 (PhC1-C6), 160.9 (HC = N), 169.6 (OCNN), 154.4, 130.6, 127.4, 125.2 (PhC9-C12), 34.9, 31.3 (C(CH$_3$)$_3$), 22.2 (SnBuCα,

$^{1}J[^{119}Sn\text{-}^{13}C]$ = 604, 578 Hz), 26.9 (SnBuCβ, $^{2}J[^{119}Sn\text{-}^{13}C]$ = 35 Hz), 26.5 (SnBuCγ, $^{3}J[^{119}Sn\text{-}^{13}C]$ = 88 Hz), 13.6 (SnBuCδ).

*Diphenyltin(IV) [N′-(2-oxidobenzylidene)-N-(oxido-(4-tert-butylphenyl)methylene)hydrazine] (**4**)*

Yield: 1.4 g, 82%; m.p. 151–153 °C; elemental analysis (%), calcd. for $C_{30}H_{28}N_2O_2Sn$: C, 63.52; H, 4.98; N, 4.94. Found: C, 63.49; H, 5.01; N, 4.91. FT-IR (KBr) υ_{max}/cm^{-1}: 1608 (m, C=N), 1071 (w, N–N), 565 (w, Sn–O), 462 (w, Sn–N). EI-MS, m/z (%): $[M]^+$ 568(60.8); $[M\text{-}2Ph]^+$ 414(2.2); $[SnPh]^+$ 197(32.4); $[tert\text{-}BuPhCO]^+$ 161(100.0); $[Sn]^+$ 120(8.9). ^{1}H NMR ($CDCl_3$ ppm): 6.80 (d, 1H, PhC2-H, $^{3}J_{H\text{-}H}$ = 8.4 Hz), 7.36 (t, 1H, PhC3-H, $^{3}J_{H\text{-}H}$ = 7.8 Hz), 6.76 (t, 1H, PhC4-H, *J* = 7.4 Hz), 7.15 (d, 1H, PhC5-H, $^{3}J_{H\text{-}H}$ = 8.1 Hz), 8.79 (s, 1H, CH = N, $^{3}J(^{119}Sn\text{-}^{1}H)$ = 52 Hz), 8.23 (d, 2H, PhC10,10′-H, $^{3}J_{H\text{-}H}$ = 8.7 Hz), 7.55 (d, 2H, PhC11,11′-H, $^{3}J_{H\text{-}H}$ = 8.7 Hz), 1.42 (s, 9H, $C(CH_3)_3$), 7.92-7.96 (m, 4H, SnPhCβ-H), 7.40–7.50 (m, 6H, SnPhCγ,δ-H), ^{13}C NMR ($CDCl_3$ ppm): 167.2, 135.3, 134.3, 122.1, 117.5, 116.9 (PhC1-C6), 161.2 (HC=N), 169.2 (OCNN), 154.8, 130.5, 127.7, 125.3 (PhC9-C12), 35.0, 31.2 ($C(CH_3)_3$), 139.2 (SnPhCα), 136.3 (SnPhCβ, $^{2}J[^{119}Sn\text{-}^{13}C]$ = 54 Hz), 128.9 (SnPhCγ, $^{3}J[^{119/117}Sn\text{-}^{13}C]$ = 83 Hz), 130.4 (SnPhCδ, $^{4}J[^{119}Sn\text{-}^{13}C]$ = 21 Hz).

*Di-n-octyltin(IV) [N′-(2-oxidobenzylidene)-N-(oxido-(4-tert-butylphenyl)methylene)hydrazine] (**5**)*

Yield: 1.4 g, 75%; m.p. viscous liquid; elemental analysis (%), calcd. for $C_{34}H_{52}N_2O_2Sn$: C, 63.86; H, 8.20; N, 4.38. Found: C, 63.89; H, 8.18; N, 4.41. FT-IR (KBr) υ_{max}/cm^{-1}: 1606 (m, C = N), 1070 (w, N–N), 566 (w, Sn–O), 463 (w, Sn–N). EI-MS, m/z (%): $[M]^+$ 640(40.6); $[M\text{-}Oct]^+$ 527(28.3); $[M\text{-}2Oct]^+$ 414(34.9); $[HSnOct]^+$ 234(5.2); $[tert\text{-}BuPhCO]^+$ 161(87.8); $[Sn]^+$ 120(3.3); $[Bu]^+$ 57(100.0). ^{1}H NMR ($CDCl_3$ ppm): 6.81 (d, 1H, PhC2-H, $^{3}J_{H\text{-}H}$ = 8.4 Hz), 7.34 (t, 1H, PhC3-H, $^{3}J_{H\text{-}H}$ = 7.5 Hz), 6.74 (t, 1H, PhC4-H, $^{3}J_{H\text{-}H}$ = 7.5 Hz), 7.18 (d, 1H, PhC5-H, $^{3}J_{H\text{-}H}$ = 8.1 Hz), 8.77 (s, 1H, CH = N, $^{3}J(^{119}Sn\text{-}^{1}H)$ = 42 Hz),8.04 (d, 2H, PhC10,10′-H, $^{3}J_{H\text{-}H}$ = 8.7 Hz), 7.47 (d, 2H, PhC11,11′-H, $^{3}J_{H\text{-}H}$ = 8.4 Hz), 1.38 (s, 9H, $C(CH_3)_3$), Hα: 1.65-1.77 (m, 4H, SnOctCα-H), 1.53-1.58 (m, 4H, SnOctCβ-H), 1.23-1.29 (br, 16H, SnOctCγ-γ′-H), 0.88 (t, 6H, SnOctδ′, $^{3}J_{H\text{-}H}$ = 6.6 Hz), ^{13}C NMR ($CDCl_3$ ppm): 166.9, 134.9, 134.1, 121.6, 117.0, 116.8 (PhC1-C6), 160.8 (HC=N); 169.6 (OCNN); 154.4, 130.6, 127.8, 125.1 (PhC9-C12), 34.9, 31.2, ($C(CH_3)_3$), 22.7 (SnOctCα, $^{1}J[^{119}Sn\text{-}^{13}C]$ = 592 Hz) 24.7 (SnOctCβ $^{2}J[^{119}Sn\text{-}^{13}C]$ = 36 Hz), 33.4 (SnOctCγ, $^{3}J[^{119}Sn\text{-}^{13}C]$ = 76 Hz), 29.2 (SnOctCδ), 29.1 (SnOctCα′), 31.2 (SnOctCβ′), 22.5 (SnOctCγ′), 14.1 (SnOctCδ′).

*Di-tert-butyltin(IV) [N′-(2-oxidobenzylidene)-N-(oxido-(4-tert-butylphenyl)methylene) hydrazine] (**6**)*

Yield: 1.3 g, 80%; m.p. 137–138 °C; elemental analysis (%), calcd. for $C_{26}H_{36}N_2O_2Sn$: C, 59.22; H, 6.88; N, 5.31. Found: C, 59.19; H, 6.91; N, 5.28. FT-IR (KBr) υ_{max}/cm^{-1}: 1606 (m, C=N), 1075 (w, N–N), 566 (w, Sn–O), 458 (w, Sn–N). EI-MS, m/z (%): $[M]^+$ 528(5.4); $[M\text{-}2tert\text{-}Bu]^+$ 414(19.9); $[Sn(tert\text{-}Bu)_2]^+$ 234(3.3); $[tert\text{-}BuPhCO]^+$ 161(21.5); $[Sn]^+$ 120(2.2); $[Bu]^+$ 57(100.0). ^{1}H NMR ($CDCl_3$ ppm): 6.86 (d, 1H, PhC2-H, $^{3}J_{H\text{-}H}$ = 8.1 Hz), 7.34 (t, 1H, PhC3-H, $^{3}J_{H\text{-}H}$ = 7.8 Hz), 6.72 (t, 1H, PhC4-H, $^{3}J_{H\text{-}H}$ = 7.5 Hz), 7.18 (d, 1H, PhC5-H, $^{3}J_{H\text{-}H}$ = 7.8 Hz), 8.80 (s, 1H, CH = N, $^{3}J(^{119}Sn\text{-}^{1}H)$ = 39 Hz), 8.09 (d, 2H, PhC10,10′-H, $^{3}J_{H\text{-}H}$ = 8.7 Hz), 7.49 (d, 2H, PhC11,11′-H, $^{3}J_{H\text{-}H}$ = 8.4 Hz), 1.38 (s, 9H, $C(CH_3)_3$), 1.36 (s, 18H, Sn-*tert*-BuCβ-H, $^{3}J(^{119/117}Sn\text{-}^{1}H)$ = 109, 104 Hz). ^{13}C NMR ($CDCl_3$ ppm): 168.0, 134.7, 133.9, 121.7, 117.0, 116.5 (PhC1-C6), 160.7 (HC=N); 169.4 (OCNN); 154.3, 130.8, 127.4, 125.2 (PhC9-C12), 34.9, 31.3, ($C(CH_3)_3$), 40.4 (Sn-*tert*-BuCα, $^{1}J[^{119/117}Sn\text{-}^{13}C]$ = 584 Hz), 29.7 (Sn-*tert*-BuCβ).

n-Butylchloridetin(IV) [*N′*-(2-oxidobenzylidene)-*N*-(oxido-(4-tert-butylphenyl) methylene)hydrazine] (**7**)

Yield: 1.2 g, 77%; m.p. 143–144 °C; elemental analysis (%), calcd. for $C_{22}H_{27}ClN_2O_2Sn$: C, 52.26; H, 5.38; N, 5.54. Found: C, 52.23; H, 5.34; N, 5.53. FT-IR (KBr) υ_{max}/cm^{-1}: 1609 (m, C=N), 1072 (w, N–N), 570 (w, Sn–O), 461 (w, Sn–N). EI-MS, m/z (%): $[M]^+$ 506(13.9); $[M\text{-}BuCl]^+$ 414(7.6); $[C_7H_4NOSn]^+$ 238(2.5); $[tert\text{-}BuPhCO]^+$ 161(100.0); $[Sn]^+$ 120(5.1); $[Bu]^+$ 57(31.8). ^{1}H NMR ($CDCl_3$ ppm): 6.84 (d, 1H, PhC2-H, $^{3}J_{H\text{-}H}$ = 8.1 Hz), 7.36 (t, 1H, PhC3-H, $^{3}J_{H\text{-}H}$ = 8.1 Hz), 6.82 (t, 1H, PhC4-H, $^{3}J_{H\text{-}H}$ = 7.2 Hz), 7.20 (d, 1H, PhC5-H, $^{3}J_{H\text{-}H}$ = 7.8 Hz), 8.86 (s, 1H, CH = N), 8.01 (d, 2H, PhC10,10′-H, $^{3}J_{H\text{-}H}$ = 8.4 Hz), 7.52 (d, 2H, PhC11,11′-H, $^{3}J_{H\text{-}H}$ = 8.4 Hz), 1.32 (s, 9H, $C(CH_3)_3$), 1.76–1.84 (m, 4H, SnBuCα-H), 1.61–1.67 (m, 4H, SnBuCβ-H), 1.45–1.57 (m, 4H, SnBuCγ-H), 0.97 (t, 6H, SnBuCδ-H, *J* = 7.2 Hz) ^{13}C NMR ($CDCl_3$ ppm): 165.9, 135.0, 134.6, 122.1, 118.0, 117.1 (PhC1-C6), 158.1 (HC=N); 166.6 (OCNN); 154.7, 130.6, 127.5, 125.7 (PhC9-C12), 35.2, 31.4 ($C(CH_3)_3$), 25.6 (SnBuCα), 28.8 (SnBuCβ), 27.4 (SnBuCγ), 14.1 (SnBuCδ).

Antibacterial activity

The antibacterial action of synthesized compounds was assessed against *Escherichia coli* ATCC 11229, *Bacillus subtilis* ATCC 11774, *Shigella flexneri* ATCC 10782, *Staphylococcus aureus* ATCC 25923, *Pseudomonas aeruginosa* ATCC 10245, and *Salmonella typhi* ATCC 10749, by agar well diffusion method. Imipenem was used as standard drug (Rehman et al. 2008). Six mm diameter wells were dug in the media by means of sterile metallic borer. Eight-hour-old

bacterial inoculums containing approximately 10^4–10^6 CFU/mL were spread over the surface of nutrient agar with the help of sterile cotton swab. The test samples with a concentration of 2 mg/mL in DMSO were introduced into the wells. Reference antibacterial drug and DMSO served as positive and negative controls, respectively. After incubation at 37°C for 20 h, the zones of inhibition (mm) were measured and compared with the standard drug.

Antifungal activity

The agar tube dilution test was used to investigate the in vitro antifungal activity of synthesized compounds against six fungal strains [*Trichophyton longifusus* ATCC 22397, *Candida albicans* ATCC 2192, *Aspergillus flavus* ATCC 1030, *Microsporum canis* ATCC 9865, *Fusarium solani* ATCC 11712, and *Candida glabrata* ATCC 90030 (Atta-ur-Rahman and Thomsen 2001). Reference drugs Miconazole and Amphotericin B were used for comparison. DMSO solutions of synthesized compounds (200 mg/mL) were prepared. The Sabouraud dextrose agar media (4 mL) prepared by mixing Sabouraud (32.5 g), glucose agar (4%), and agar–agar (20 g) in 500 mL of distilled water was dispensed into screw-capped tubes and autoclaved for 15 min at 121 °C. The prepared test compound solutions were added to non-solidified Sabouraud agar media (50 °C). This was then solidified at room temperature and inoculated with 4 mm diameter portion of inoculums, derived from a 7-day-old respective fungal culture. An agar surface streak was employed to ensure non-mycelial growth. The tubes were incubated at 27–29°C for 7–10 days and the growth inhibition was measured with reference to the control.

Cytotoxicity

The cytotoxicity of the synthesized compounds was investigated by the Brine shrimp lethality test (Atta-ur-Rahman and Thomsen 2001). Brine shrimps (*Artemia salina*) eggs were hatched in a vessel containing sterile simulated seawater, prepared using 38 $g.L^{-1}$ sea salt; pH was adjusted to 8.5 using 1 M NaOH at room under constant aeration, for 2 days. Thirty active nauplii were placed in a vial containing brine solution (4.5 mL) and a drop of yeast suspension. In each experiment, test solution (0.5 mL) was added to the vial and surviving larvae were counted at ambient temperature after 24 h. Experiments were conducted in triplicate for each concentration (1, 10, and 100 mg/mL) of test substances and compared with the control. Data were analyzed with Finney's probit analysis to determine the LD_{50} (Finney 1971). Etoposide was used as the standard drug.

Computational details

The present quantum chemical calculations have been performed using the DFT method employing B3LYP hybrid functional as implemented in the Gaussian 09 software (Becke 1988; Frisch et al. 2009; Lee et al. 1988). A graphical user interface, GaussView 5, was used to prepare input files as well as to visualize/plot the theoretical results (Dennington et al. 2009). Geometry optimization and harmonic frequency calculations were carried out for isolated gas phase $\mathbf{H_2L}$ compound and seven new diorganotin (IV) complexes in the ground electronic state at B3LYP/6-311 ++G(d,p) level and B3LYP/6-311 ++G(d,p)/LANL2DZ level of theory, respectively. The basis set LANL2DZ with effective core potential was chosen for Sn atom while for other atoms (C, H, N, O, and Cl) 6-311 ++G(d,p) basis set was used. The lack of imaginary values in the calculated wavenumbers revealed the optimized geometry corresponding to an energy minimum on potential energy surface. The harmonic frequencies generally overestimate the experimental one mainly by ignoring anharmonic terms in potential energy expression. This overestimation appears systematically. Therefore, various types of scaling factors have been employed to match theoretical IR band position with experimental one. In this work, a uniform scaling factor, 0.960 in the high wavenumbers region and by 0.988 in the low wavenumbers region (below 1800 cm^{-1}), was used to scale down the harmonic wavenumbers (Borba et al. 2010). The IR spectra of the compounds were simulated using Lorentzian band shape with FWHM of 5 cm^{-1}. The NMR spectra (^1H and ^{13}C) of the present compounds were simulated in the solvent phase (chloroform) using gauge independent atomic orbital (GIAO) method within DFT/B3LYP framework. The integral equation formalism (IEF) version of the polarizable continuum model (IEF-PCM) was employed for the NMR spectra calculations in the solvent phase. Each solvent-phase optimized structure of the present ligand as well as complexes was subjected to single point GIAO-NMR calculations in a polarized continuum of chloroform. Relative chemical shift values (in ppm) were obtained by subtracting the corresponding tetramethylsilane (TMS) shielding for ligand at GIAO-B3LYP/6-311 + G(2d,p) and complexes at GIAO-B3LYP/6-311 + G(2d,p)/LANL2DZ level of theory. Furthermore, various other molecular properties such as atomic charges, dipole moment, chemical reactivity descriptors based on highest occupied molecular orbital (HOMO) and lowest unoccupied molecular orbital (LUMO), molecular electrostatic potential (MEP), thermodynamic properties, and HOMO–LUMO analysis of the ligand, as well as complexes were also reported.

Results and discussion

The condensation of salicylaldehyde with 4-tert-butylbenzoic hydrazide in ethanol afforded the ligand N′-(2-hydroxybenzylidene)-4-*tert*-butylbenzohydrazide (**H_2L**), which, on reaction with diorganotin(IV) compounds in stoichiometric ratio, yielded R_2SnL (**1–6**) (R=–CH_3, –C_2H_5, -*n*-C_4H_9, –C_6H_5, –C_8H_{17}, -tert-C_4H_9) and BuClSnL (**7**) in good yield (75–88%, Scheme 1, 2). All the compounds are stable in air at room temperature, soluble in common organic solvents and solids under normal conditions except compound (**5**). The elemental analysis data provided in the experimental section support the formation of complexes and suggest a 1:1 diorganotin(IV) and ligand ratio.

Infrared spectroscopy

Comparison of IR spectra of complexes with the free ligand helps in the identification of characteristic vibrational frequencies and gives an insight into the binding modes of ligand and structure of complexes formed. In FT-IR spectrum of ligand, the bands observed at 3455 and 3178 cm^{-1} are assigned to νOH and νNH stretching vibrations respectively, whereas the corresponding theoretical wavenumbers are 3292 and 3388 cm^{-1} respectively. Theoretically, O–H stretching wavenumber is predicted at lower region than N–H stretching wavenumber due to consideration of intramolecular interaction (O–H—N) only in calculation. The H_2L compound is appeared with its dimer structure in crystal having interactions, O–H—N (intramolecular) and C=O–H–N (intermolecular). Therefore, the frequencies of O–H, N–H, and C=O stretching vibrations are shifted considerably towards lower region. A sharp band at 1669 cm^{-1} indicates the presence of C=O group and existence of ligand in the amido form. The corresponding theoretical IR frequency is found to be 1729 cm^{-1}. The absence of all these bands in the IR spectra of complexes suggests that during complex formation, the ligand undergoes tautomeric shift from amido to enolic form followed by deprotonation and coordination to diorganotin(IV) moieties. The absorption band due to νC=N in ligand observed at 1616 cm^{-1} shifts to lower values in the spectra of all diorganotin (IV) complexes indicating shifting of electron density from the nitrogen of C=N group to tin atom or coordination of azomethine nitrogen with the tin center (Pettinari et al. 2001). Furthermore, this causes a decrease in inter lone-pair repulsion on the nitrogen atoms and shifts the υ(N–N) frequencies to higher values at 1070–1080 cm^{-1} in the spectra of organotin(IV) complexes. These IR frequencies are also found in accordance with theoretical values. The band due to C=N stretching vibration in ligand is predicted at 1648 cm^{-1}, while in all tin complexes, this vibration is appeared comparatively at lower value around 1613 cm^{-1}. The N–N stretching vibration is predicted within the region 1030–1050 cm^{-1} for the tin complexes, whereas this vibration is found 1158 cm^{-1} for **H_2L** compound. In all the synthesized complexes, new IR bands also emerge in the regions of 559–570 cm^{-1} and 451–458 cm^{-1} due to the formation of Sn–O and Sn-N bonds, respectively (Hong et al. 2011; Muhammad et al. 2012). The corresponding theoretical IR bands due to Sn–O and Sn–N stretching vibrations are occurred in the regions 615–605 cm^{-1} and 575–560 cm^{-1}, respectively. The appearance of these absorption bands supports the formation of complexes. Even after scaling the IR frequencies, the values are found larger than those of experimental one due to the fact that calculations have been carried out for the isolated molecule in the gaseous phase, while the experiments belong to solid phase.

NMR spectroscopy

The comparison of ^{1}H NMR spectrum of ligand and diorganotin (IV) complexes indicates some explicit structural changes in the ligand and also provides useful information regarding the binding mode of ligand. The disappearance of resonance signals due to OH and NH groups in the ^{1}H NMR spectra of all diorganotin(IV) complexes **1-7** indicates that the ligand undergoes enolization and deprotonation before forming the organotin(IV) complexes (Shujah et al. 2013). The proton and carbon (^{13}C) NMR spectra of ligand as well as all complexes obtained by GIAO-DFT/B3LYP method have been compared with the experimental one and are found in good agreement.

The aromatic protons of the ligand and methyl protons of tert-butyl group give signal in the region δ 6.92–7.30 and 1.32 ppm, respectively, whereas theoretically, the proton NMR signals occurred around 7–8 ppm and 1–2 ppm, respectively. Since these groups are not involved in bonding, so all these signals remain unaffected in the NMR spectra of diorganotin(IV) complexes.

The azomethine proton (CH = N) gives a signal at 8.64 ppm, while theoretically, it appeared at 8.41 ppm (in **H_2L**). In all the diorganotin(IV) complexes, a downfield shift to 8.76–8.80 ppm and appearance of tin satellite with $^3J(^{119}Sn\text{-}^1H)$ spin–spin coupling constant of 39 - 52 Hz indicate the shifting of electron density from azomethine nitrogen to Sn atom and presence of Sn-N coordinated bond in solution. The chemical shifts and coupling constants are consistent with reported diorganotin(IV) complexes of ONO donor type ligands (Shujah et al. 2011). The diorganotin(IV) complexes show additional signals owing to the protons of alkyltin(IV) moieties. The CH_3 protons in complex (**1**) resonate as a singlet at 0.85 ppm (around 0.5 ppm in theoretical H-NMR spectrum) with Sn satellites corresponding to $^2J(^{119}Sn\text{-}^1H)$ coupling constants of 79 Hz. The $^2J(^{119}Sn, ^1H)$ coupling constant is a valuable parameter used to estimate

Table 1 (C-Sn–C) angles (◦) based on NMR parameter of selected organotin(IV) complexes

Comp. no.	$^{1}J(^{119}Sn, ^{13}C)$ (Hz)	$^{2}J(^{119}Sn, ^{1}H)$ (Hz)	Angle (◦)	
			θ (^{1}J)	θ (^{2}J)
1	655	79	134.2	129.6
2	618	–	131.0	–
3	604	–	135.3	–
5	592	–	134.1	–
6	584	–	133.4	–

Me–Sn–Me bond angle in solution state. In the present study, only the dimethyltin(IV) derivative exhibits $^{2}J(^{119}Sn, ^{1}H)$ coupling in solution. On substitution the value of ^{2}J in Lockhart's equation $\theta = 0.0105\,[^{2}J]^{2} - 0.799[^{2}J] + 122.4$, we get θ, the Me-Sn-Me angle, equal to 129.6° indicating a pentacoordinated tin atom in solution (Lockhart and Manders 1986). The terminal methyl of diethyl, dibutyl, dioctyl, and butylchlorotin(IV) complexes (**2**), (**3**), (**5**), and (**7**) appear as triplet at 1.32, 0.90, 0.88, and 0.97 ppm with a $^{3}J(^{1}H\text{-}^{1}H)$ coupling constant 7.2, 7.2, 6.6, and 7.2 Hz, respectively. Rest of the protons resonate in the expected range. In complex (**6**), the *tert*-butyl protons resonate at 1.36 ppm as singlet with a $^{3}J(^{117/119}Sn\text{-}^{1}H)$ coupling constant of 104 and 109 Hz. The protons of diphenyltin moiety in complex (**4**) appear as multiplets in the regions 7.92–7.96 and 7.40–7.50 ppm. The ^{13}C NMR spectra data of complexes show a downfield shift of all carbon resonances, compared with that of the ligand, because coordination leads to the shifting of electron density from the ligand to diorganotin(IV) moieties. For organotin(IV) compounds, the ^{1}J [^{119}Sn, ^{13}C] coupling constants are important parameters used to evaluate the molecular structure and establish the coordination around tin in solution. Among the synthesized complexes $^{1}J(^{119}Sn, ^{13}C)$ coupling satellites were observed only for compounds 1, 2, 3, 5, and 6. The C–Sn–C bond angles in solution based on $^{1}J(^{119}Sn, ^{13}C)$ coupling constants have been calculated

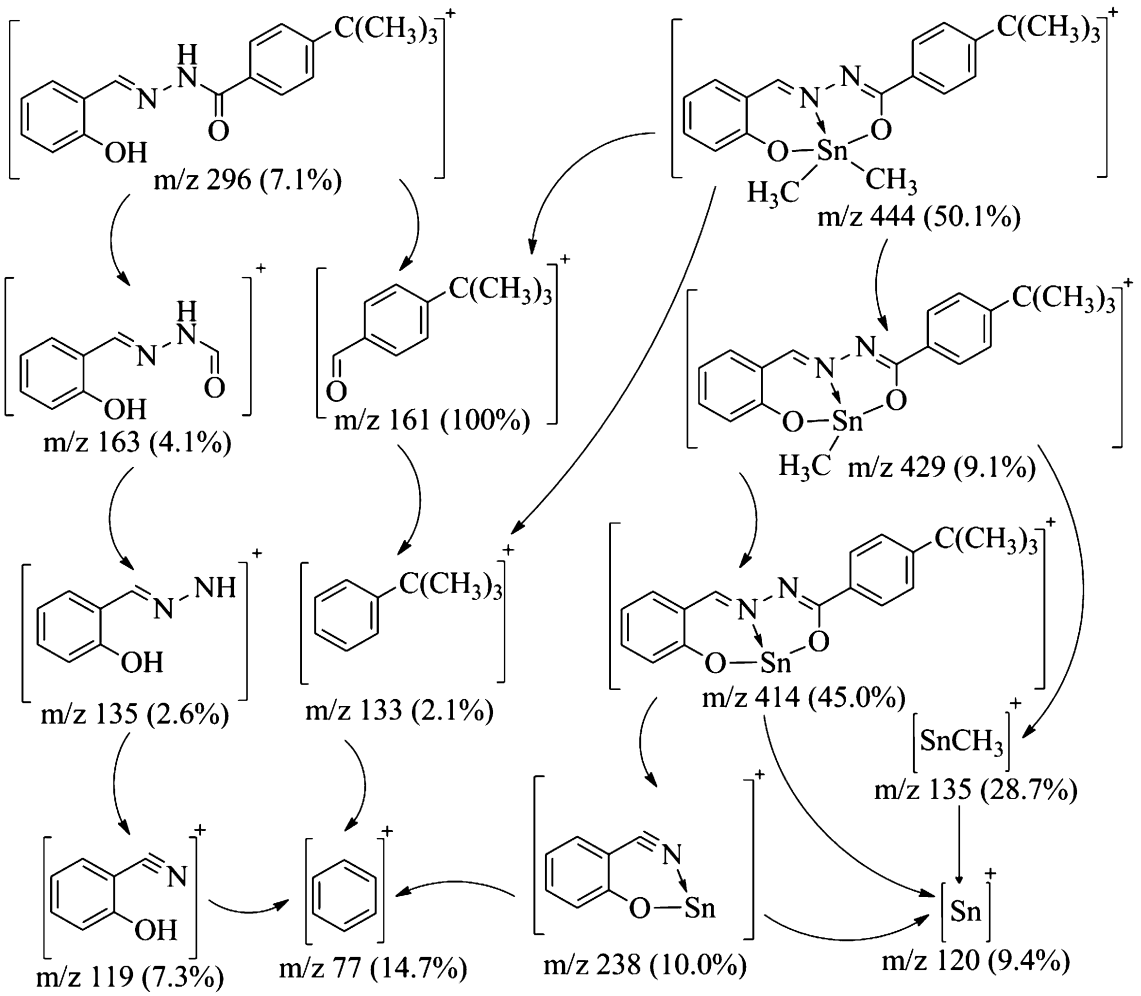

Scheme 3 Proposed mass fragmentation pattern of ligand (H_2L) and dimethyltin(IV) complex (1)

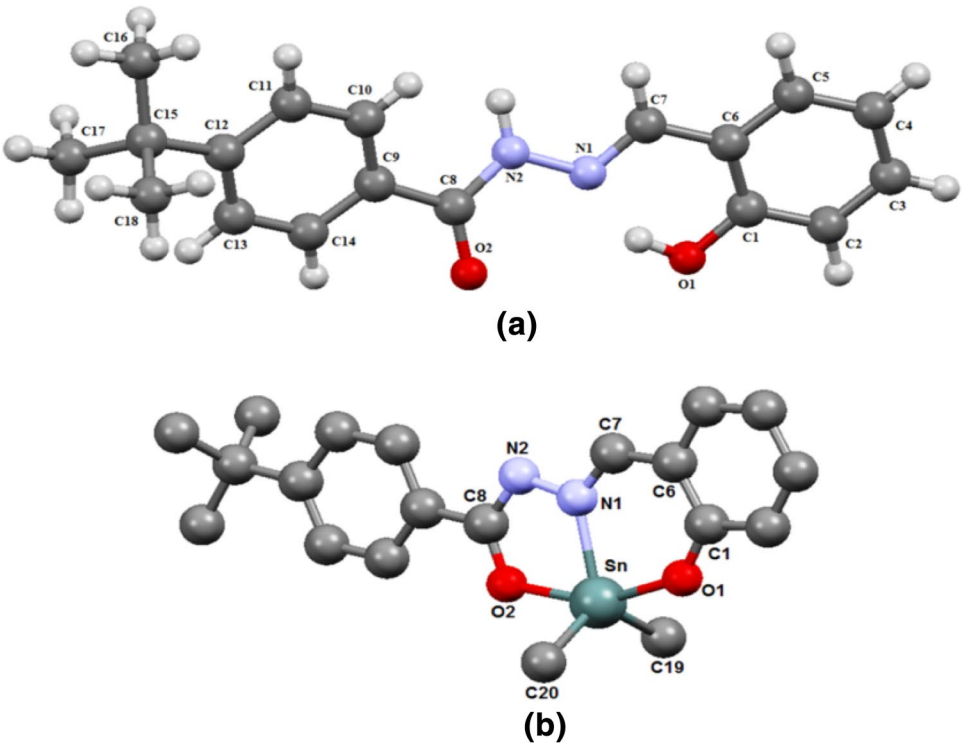

Fig. 1 Molecular structure of ligand (**a**) and optimized structure of dimethyltin(IV) complex (**b**) with the atomic numbering scheme

and results reported in Table 1. The coupling constants for compounds (**1**), (**2**), (**3**), (**5**), and (**6**) were found to be in the range 584–655 Hz, which suggest pentacoordination around Sn atom in solution (Holeček and Lyčka 1986).

Mass spectrometry

The EI-MS spectral data of ligand (H_2L) and diorganotin(IV) complexes (R_2SnL, **1**–**7**) are provided in the experimental section. The molecular ion peak and fragments containing tin were recognized on the basis of unique peak pattern attributed to ten stable isotopes of tin. The molecular ion $(C_{18}N_{18}N_2O_2SnR_2)^{+\cdot}$ is observed in all cases; however, the peak intensity is low in case of complex (**6**) and (**7**). The first fragmentation step involves the formation of $(C_{18}N_{18}N_2O_2SnR_2)^{+\cdot}$ fragment due to the loss of R group (R = CH_3, C_2H_5, C_4H_9, C_8H_{17} except for complex (**4**) and (**7**) where the loss of both R leads to the formation of $(C_{18}N_{18}N_2O_2Sn)^{+\cdot}$. The fragments $((CH_3)_3CC_6H_4CO)^{+\cdot}$ and $(C_4H_9)^{+\cdot}$ are base peaks for H_2L, (**1**), (**2**), (**3**), (**4**), (**7**), and **5**, **6,** respectively. In addition, RSn^+ and Sn^+ ions of significant peak intensity are also observed for all the complexes (**1**–**7**). The mass spectral data for the fragmented ions are in close agreement with the proposed structure of the diorganotin(IV) complexes. The proposed fragmentation pattern of ligand and dimethyltin(IV) complex is provided in Scheme 3.

X-ray crystal structure of *N′*-(2-hydroxybenzylidene)-4-tert-butylbenzohydrazide (H_2L)

The molecular structure along with the atomic numbering scheme for ligand (**H_2L**) is shown in Fig. 1. Crystal parameters, selected bond lengths, and bond angles are given in Tables 2 and 3 respectively. The asymmetric unit of title compound consists of one molecule. In the solid state, the compound exists in the amido form, carbonyl and phenolic –OH groups are retained in the *cis* position. The N(1)-C(7) and O(2)-C(8) bond lengths [1.288(2), 1.243(2) Å] indicate their double bond nature. However, the N(1)–N(2), N(2)–C(8), and O(1)-C(1) bond lengths [1.381(2), 1.354(3), and 1.362(3) Å] support their single bond nature. Rest of the bond lengths are in the normal range. In the solid state, supramolecular architecture is formed mediated by N(2)-H···O(2) and C-H…π interactions (Fig. 2). The data relating to hydrogen bonds are depicted in Table 4.

Optimized molecular geometry

The comparison of optimized structural parameters (bond lengths and bond angles) with the XRD data of **H_2L** compound has been presented in Table 3. The synthesis scheme of the **H_2L** compound has two possibility of product namely T1 and T2 (Scheme 1). The optimized geometries of isolated **H_2L** compound (T1 and T2) with numbering scheme are illustrated in Fig. 3. The self-consistent field (SCF) minimum energy on the potential energy surface (PES) of T1 and

Table 2 Crystal data and structure refinement parameters for ligand (H_2L)

Empirical formula	$C_{18}H_{20}N_2O_2$
Formula mass	296.37
Crystal system	Orthorhombic
Space group	*Pbca*
a (Å)	13.982(4)
b (Å)	9.269(3)
c (Å)	24.557(7)
α(°)	90.00
β(°)	90.00
γ(°)	90.00
V (Å^3)	3182.6 (16)
Z	8
Crystal habit	Needle
Size (mm)	0.61 × 0.20 × 0.14
T (K)	100 (1)
ρ (g.cm^{-3})	1.237
μ (Mo Kα) (cm^{-1})	0.81
F(000)	1264
Total reflections	14719
Independent reflections	3234
For ($F_o \geq 4.0\ \sigma\ (F_o)$)	1946
$R(F) = \Sigma(\|\|F_o\| - \|F_c\|\|)/\Sigma\|F_o\|$ For $F_o > 4.0\ \sigma\ (F_o)$	0.0486
$wR(F^2) = [\Sigma[w(F_o^2 - F_c^2)^2]/\Sigma[w(F_o^2)^2]]^{1/2}$	0.1264
Goodness-of-fit	1.007
θ Range (deg)	3.12–26.72
Data/restrictions/params	3234/0/279
Largest diff. peak and hole (eÅ^{-3})	−0.19 and 0.23(5)

Table 3 Comparison of optimized structural parameters [bond lengths (Å) and bond angles (°)] with the XRD data of **H_2L** compound

Bond lengths	Experimental	B3LYP/6-311 ++G(d,p)
O(1)–C(1)	1.362(3)	1.344
O(2)–C(8)	1.243(2)	1.214
N(1)–N(2)	1.381(2)	1.357
N(1)–C(7)	1.288(3)	1.286
N(2)–C(8)	1.354(3)	1.389
C(8)–C(9)	1.486(3)	1.498
Bond angles		
N(2)–N(1)–C(7)	116.96(16)	118.9
N(1)–N(2)–C(8)	118.04(16)	120.3
O(1)–C(1)–C(2)	117.46(18)	117.7
O(1)–C(1)–C(6)	122.16(18)	122.9
N(1)–C(7)–C(6)	120.12(17)	121.6
O(2)–C(8)–N(2)	122.33(18)	122.4
O(2)–C(8)–C(9)	120.95(17)	123.1
N(2)–C(8)–C(9)	116.70(16)	114.5

T2 is found to be −601262.145 and −601258.786 kcal/mol respectively at B3LYP/6-311 ++G(d,p) level of theory. The minimum molecular energy has been obtained for T1 geometry (with N–H); therefore, it is found more stable than T2 geometry. This has been also confirmed from geometry (T1) of **H_2L** molecule obtained by XRD. The further theoretical investigations have been carried out on optimized geometry of T1. The optimized geometries of other seven new complexes have been also presented in Fig. 4.

Calculated geometric parameters of the present diorganotin(IV) complexes are summarized in Table 5. The 6-311 ++G(d,p) basis set led calculations of bond lengths and bond angles are comparable to reported experimental data in one of our research articles (Shujah et al. 2011).

In diorganotin(IV) complexes, the tin atom is present in a strongly distorted square-pyramidal geometry. In complexes (1–7), the distortions in bond lengths and angles of optimized geometry obtained at DFT/B3LYP from a possible geometry (Shujah et al. 2011) are found respectively around 0.1Å and 1–4°.

Other theoretical molecular parameters

Various important molecular parameters such as molecular energy, dipole moment, thermodynamic parameters, HOMO–LUMO energy eigen values, HOMO–LUMO energy gaps, and global reactivity descriptors of the ligand, as well as complexes have been depicted in Table 6. The dipole moment values for complexes 1–5 and 7 are found to be around zero as these molecules have center of symmetry. The HOMO and LUMO are the main molecular orbitals which are involved in charge transfer within the molecule. The HOMO shows the ability to donate an electron, while LUMO exhibits the capability to accept an electron. The energy eigen values of HOMO and LUMO are directly related to ionization potential and electron affinity, respectively. The energy gap between HOMO and LUMO determines the kinetic stability and chemical reactivity of molecule. The plots of frontier molecular orbitals (HOMO and LUMO) for H_2L and complexes (1–7) are shown in Fig. 5. These plots show the charge transfer through conjugated pi bonds as well as through Sn connected bonds. The low HOMO–LUMO gap estimated around 4 eV for H2L compound and around 3.5 eV for the complexes (1–7) shows the significant degree of intramolecular charge transfer, high chemical reactivity, and low kinetic stability. The global reactivity descriptors related to HOMO–LUMO energy eigen values of the present molecules obtained at DFT level, such as hardness, softness, chemical potential, and electrophilicities, are reported to understand their chemical reactivities. The large HOMO–LUMO gap indicates a hard molecule with low chemical reactivity, while low HOMO–LUMO energy gap shows a soft molecule of

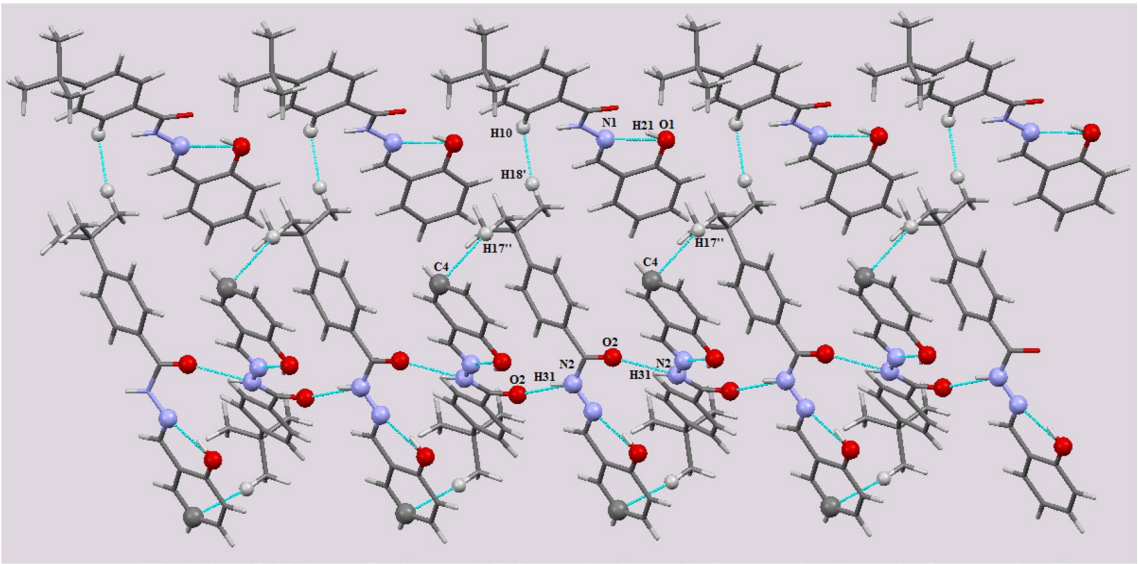

Fig. 2 Supramolecular architecture mediated by N(2)-H…O(2) and C-H…π interactions in the crystal lattice of H_2L

Table 4 Hydrogen-bond geometry (Å, °) for H_2L

D-H···A	D-H	H····· A	D····· A	D-H·····A
O(1)-H(21)···N(1)	0.93	1.79(3)	2.633(2)	149.0(3)
N(2)-H(31)···O(2)	0.938(19)	1.895(19)	2.800(2)	161.4(19)
C(7)-H(7)···O(2)	0.989(19)	2.41(2)	3.198(3)	136.3(16)
C(10)-H(10)···O(2)	0.93(2)	2.57(2)	3.412(3)	150.2(16)

high chemical reactivity. The negative chemical potentials also define the stability of molecule. The electrophilicity index measures the degree of transfer of electrons from a donor to an acceptor system. The equations used to obtain these descriptors and their significance can be found in the literature (Ayers et al. 2005; Chermette 1999; Geerlings and De Proft 2008; Geerlings et al. 2003; Kohn et al. 1996; Parr and Yang 1989, 1995). The derived reactivity indices based on HOMO and LUMO energy eigen values given in this work are for qualitative comparison purposes.

The MEP surface plot of molecule is very useful in qualitative interpretation of the electrophilic and nucleophilic reactions as well as intermolecular hydrogen-bonding interactions. MEP surface plots, generated for the present molecules by mapping of electrostatic potential on to the constant electron density surface, are shown in Fig. S10.

Antibacterial activity

All the compounds (**H_2L, 1-7**) were tested against pathogenic bacterial strains using the agar well diffusion method (Table 7). The in vitro inhibitory activity was performed against *Escherichia coli*, *Bacillus subtilis, Sigella flexneri, Staphylococcus aureus, Pseudomonas aeruginosa,* and *Salmonella typhi*, using imipenem as standard drug. The ligand showed moderate activity only against *Shigella flexneri*, Gram-negative bacteria, mainly responsible for diarrhoeal diseases in humans. The results indicate that on complexation, the antibacterial activity increases which is also supported by earlier reports (Anwer et al. 2013).

Most of the antibacterial agents are more active against Gram-positive bacteria, because they do not possess outer membrane and only have a loosely packed porous polyglycane exterior layer through which the penetration of drug into the cell is easy. However, in the present study,

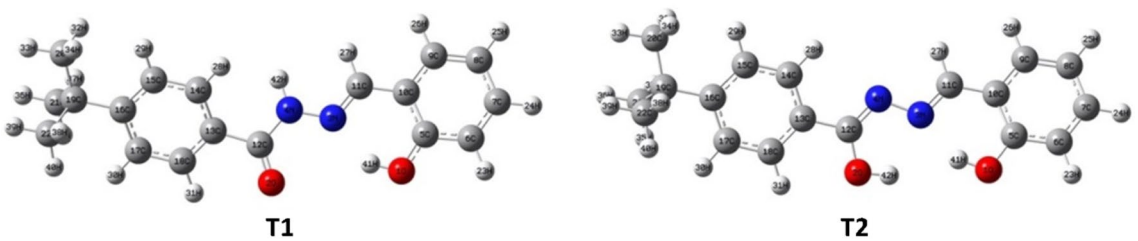

Fig. 3 Optimized geometry of two possible structure of Schiff base (H_2L) (T1 and T2) obtained at B3LYP/6-311++G(d,p) level of theory

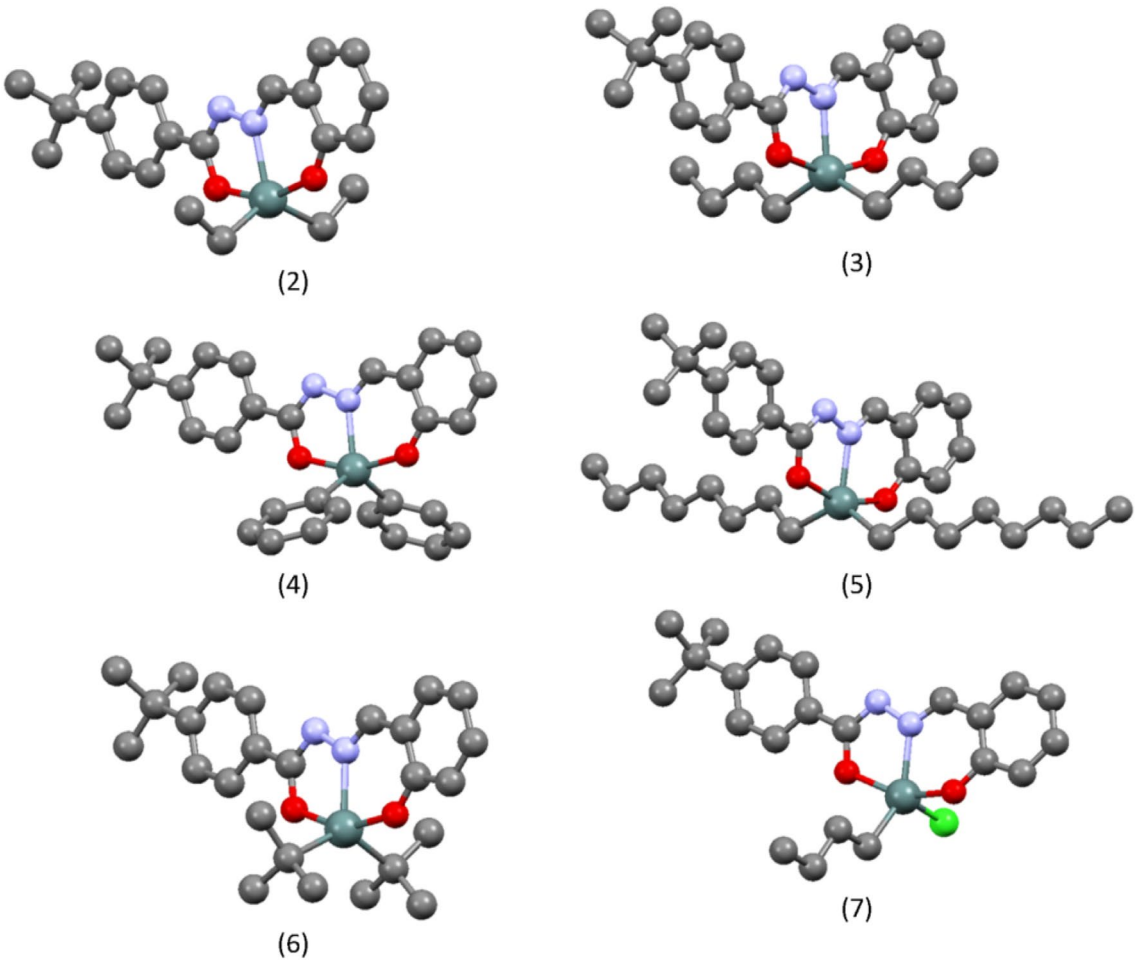

Fig. 4 Optimized structures of diorganotin(IV) complexes (2-7). Hydrogen atoms have been omitted for clarity

it was found that the synthesized compound show moderate activity against all the investigated bacterial strains, although some individual differences also existed among the tested bacteria; however, the diorganotin(IV) complexes (**1-7)** exhibited a better antibacterial activity than the ligand $\mathbf{H_2L}$. No significant difference in the antibacterial activities of complexes against Gram-positive bacteria and Gram-negative bacteria has been observed. Among the tested bacteria, *Staphylococcus aureus and Escherichia coli* were most visibly inhibited by (**4**) and (**7**), respectively. The exact mechanism of action of synthesized compounds is yet to be investigated, however, Overtone's concept and Tweedy's chelation theory, which demands a better lipophilicity for antimicrobial action can be used to rationalized the enhanced activity of complexes (Fukushima et al. 2012; Zia ur et al. 2009). None of the synthesized compounds was more active than the standard drug.

Antifungal activity

The in vitro antifungal activities of ligand $\mathbf{H_2L}$ and diorganotin(IV) complexes (**1–7**) were tested against six human pathogenic fungal strains including yeasts (*Candida albicans* and *Candida glabrata*), dermatophytes (*Microsporum canis* and *Trichophyton longifusus*), and opportunistic molds (*Aspergillus flavus* and *Fusarium solani)* using the agar tube dilution protocol. Amphotericin B and Miconazole were used as standard drug. The results are presented in Table 8. Metallation usually boosts the antifungal activity; thus, the diorganotin(IV) complexes show a noticeably high antifungal activity than the ligand. Highest activity was shown by compound (**6)** against *F. solani*. Moderate activity against *A. falvis* and *M. canis* was shown by compounds (**3**) and (**1**), respectively. All the compounds showed insignificant activity against *Trichophyton longifusus* and Candida glabrata. The mechanistic details of inhibitory action against various fungal strains are yet to be explored; however, the

Table 5 Calculated geometric parameters [bond length (Å) and bond angles (°)] of diorganotin(IV) complexes (1–7)

	(1)	(2)	(3)	(4)	(5)	(6)	(7)	Exp.
Bond lengths (Å)								
O(1)-C(1)	1.312	1.311	1.311	1.316	1.311	1.312	1.321	1.324
O(2)-C(8)	1.301	1.301	1.300	1.305	1.300	1.301	1.307	1.299
N(1)-N(2)	1.384	1.384	1.384	1.382	1.382	1.384	1.379	1.412
N(1)-C(7)	1.305	1.305	1.305	1.303	1.305	1.305	1.306	1.298
N(2)-C(8)	1.316	1.316	1.316	1.314	1.315	1.315	1.314	1.296
C(8)-C(9)	1.480	1.480	1.480	1.479	1.480	1.481	1.475	–
Sn-N(1)	2.193	2.197	2.196	2.182	2.197	2.206	2.179	2.161
Sn–O(1)	2.075	2.083	2.083	2.066	2.080	2.089	2.037	2.065
Sn–O(2)	2.116	2.126	2.127	2.110	2.128	2.135	2.081	2.145
Sn–C(19)	2.122	2.138	2.137	2.126	2.135	2.187	–	2.119
Sn–C(20)	2.122	2.138	2.137	2.126	2.137	2.187	2.124	2.122
Bond angles (°)								Exp.[a]
O(1)-Sn–O(2)	155.56	155.04	155.10	156.68	155.22	154.23	152.80	158.48
O(1)-Sn-N(1)	82.85	82.53	82.57	83.53	82.84	82.02	83.08	84.50
O(1)-Sn–C(19)	95.74	95.61	95.64	95.47	94.98	95.16	–	96.20
O(1)-Sn–C(20)	95.74	95.61	95.64	95.47	96.70	96.28	94.73	95.13
O(2)-Sn-N(1)	72.71	72.51	72.53	73.15	72.52	72.22	73.13	74.00
O(2)-Sn–C(19)	95.53	95.71	95.62	95.24	94.65	96.18	–	93.70
O(2)-Sn–C(20)	95.53	95.71	95.62	95.24	96.17	95.05	95.32	94.87
N(1)-Sn–C(19)	117.5	117.05	117.03	117.39	118.9	116.26	–	115.19

Table 6 Various theoretical molecular parameters

Parameters	H_2L	(1)	(2)	(3)	(4)	(5)	(6)	(7)
SCF Energy (kcal/mol)	− 601262.1450	− 652775.6812	− 702122.9925	− 800830.0047	− 893460.5399	− 998230.9442	− 990572.3344	− 800823.4798
Dipole moment (Debye)	6.349	0.417	0.261	0.256	0.803	0.206	3.328	0.381
ZPVE (kcal/mol)	216.531	248.016	284.322	355.389	316.020	498.178	280.057	354.077
Total thermal energy (kcal/mol)	229.425	264.566	302.469	376.960	336.216	526.537	298.613	375.646
Cv (cal/mol/K)	80.417	99.675	108.904	128.402	124.955	166.995	110.530	131.465
Total entropy, S (cal/mol/K)	152.105	182.150	194.835	223.802	211.254	280.351	199.433	215.815
E_{HOMO} (eV)	− 6.104	− 5.769	− 5.719	− 5.706	− 5.880	− 5.619	− 6.115	− 5.701
E_{LUMO} (eV)	− 1.976	− 2.232	− 2.198	− 2.186	− 2.305	− 2.078	− 2.506	− 2.194
$E_{LUMO-HOMO}$ Gap (eV)	4.128	3.537	3.521	3.520	3.575	3.541	3.609	3.507
Global reactivity descriptors (eV)								
Ionization potential (IP), i.e., -HOMO	6.104	5.769	5.719	5.706	5.880	5.619	6.115	5.701
Electron affinity (EA), i.e., -LUMO	1.976	2.232	2.198	2.186	2.305	2.078	2.506	2.194
Electronegativity (χ)	4.040	4.001	3.959	3.946	4.093	3.849	4.311	3.948
Chemical potential (μ)	− 4.040	− 4.001	− 3.959	− 3.946	− 4.093	− 3.849	− 4.311	− 3.948
Electrophilicity (ω)	3.954	4.525	4.450	4.424	4.685	4.183	5.148	4.443
Hardness (η)	2.064	1.769	1.761	1.760	1.788	1.771	1.805	1.754
Softness (S)	0.242	0.283	0.284	0.284	0.280	0.282	0.277	0.285

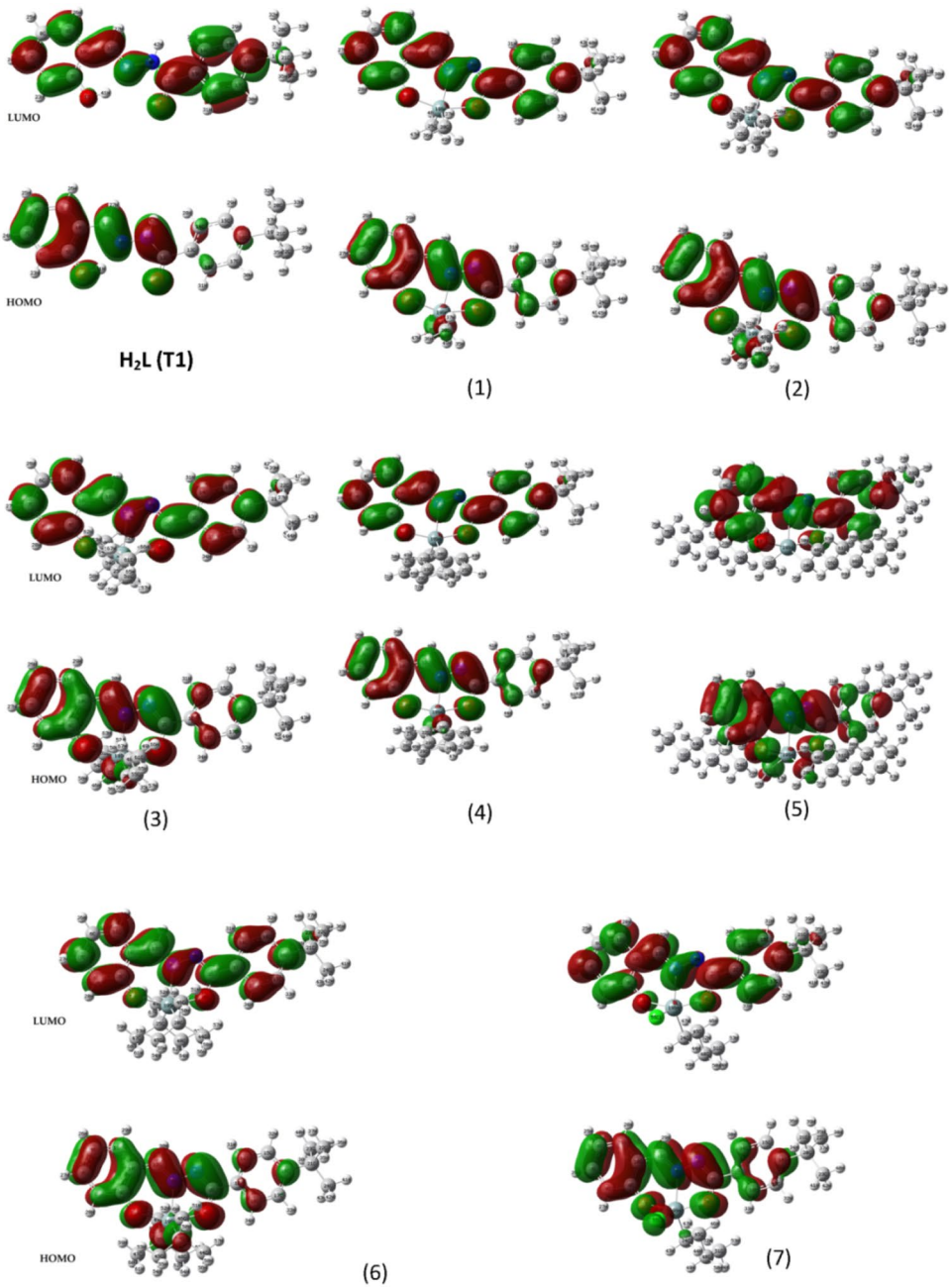

Fig. 5 HOMO–LUMO plots of Schiff base ligand (H_2L) and diorganotin(IV) complexes (1–7)

Table 7 Antibacterial activity of N′-(2-hydroxybenzylidene)-4-*tert*-butylbenzohydrazide (H_2L) and its organotin(IV) complexes

Bacterium	Inhibition zone diameter (mm)								Reference drug[b]
	H_2L	(1)	(2)	(3)	(4)	(5)	(6)	(7)	
Escherichia coli	–	14	–	15	13	–	12	16	30
Bacillus subtilis	–	–	12	15	–	–	10	11	37
Shigella flexneri	10	12	10	12	–	12	12	14	36
Staphylococcus aureus	–	11	–	10	15	–	13	–	26
Pseudomonas aeruginosa	–	10	–	8	–	10	–	–	32
Salmonella typhi	–	8	12	10	9	–	–	–	30

[a]Conc. 1 mg/mL of DMSO, [b]Reference drug, Imipenem, – Insignificant activity

Table 8 Antifungal activity[a-c] (% inhibition) of *N′*-(2-hydroxybenzylidene)-4-tert-butylbenzo hydrazide (H_2L) and its organotin(IV) complexes

Fungus	Inhibition (%)								Standard drug[c]	MIC[b] (μg/mL)
	H_2L	(1)	(2)	(3)	(4)	(5)	(6)	(7)		
Trichophyton longifusus	–	–	–	–	–	–	–	–	Miconazole	70.0
Candida albicans	–	–	–	–	–	10	–	–	Miconazole	110.8
Aspergillus flavus	20	30	–	65	40	–	60	–	Amphotericin B	20.0
Microsporum canis	30	70	60	–	–	40	–	20	Miconazole	98.4
Fusarium solani	–	20	50	–	70	30	80	–	Miconazole	73.2
Candida glabrata	–	–	–	–	–	–	–	–	Miconazole	110.8

[a]Concentration: 200 μg/mL of DMSO, [b]MIC: Minimum inhibitory concentration, [c]Percent inhibition (standard drug) = 100, – no inhibition

Table 9 Brine Shrimp (*Artemia salina*) lethality bioassay data of diorganotin(IV) derivatives of N′-(2-hydroxybenzylidene)-4-tert-butylbenzohydrazide

Sample code	(H_2L)	(1)	(2)	(3)	(4)	(5)	(6)	(7)
LD_{50} (μg/mL)	–	26.61	–	0.44	–	–	–	–

Standard drug: Etoposide, LD_{50} 7.46 μg/mL

activity of synthesized compounds can be ascribed to their potential to interact with intracellular bioreceptors' triggering disruption in the movement of ribosome and obstructing nuclear protein and DNA synthesis with in the cell (Ayoko et al. 2003; Chaudhary et al. 2009).

Cytotoxicity

The synthesized ligand **H_2L** and diorganotin(IV) complexes (**1–7**) were assessed for cytotoxicity by in vivo lethality to brine shrimp nauplii (Table 4). The ability of organotin(IV) compounds to interact with the donor sites in DNA and proteins, their potential to stimulate oxidative damage and impede ATP synthesis and ability to cause apoptosis, necrosis or blockage of estrogen receptors are the primary factors responsible for their cytotoxic character (Shpakovsky et al. 2014; Tariq et al. 2014).

Among the synthesized compound, the dibutyltin(IV) derivative (**3**) displayed highest toxicity with LD_{50} 0.44 μg/mL (Table 9), rest of the compounds does not show any significant toxicity against the Brine Shrimp (larvae).

Conclusions

Seven new diorganotin(IV) derivatives of N′-(2-hydroxybenzylidene)-4-tert-butylbenzohydrazide have been synthesized and characterized by elemental analysis, mass spectroscopy, FT-IR, multinuclear NMR (^{1}H, ^{13}C and ^{119}Sn), and DFT/B3LYP calculations. The ligand coordinates with the dialkytin(IV) moieties in the iminol form through ONO donor sites. The $^1J(^{119}Sn, ^{13}C)$ coupling constant values found were in the range 584–655 Hz and $^2J(^{119}Sn\text{-}^1H)$ coupling constants of 79 Hz for complex (**1**) suggest pentacoordination around Sn atom in solution. Single-crystal X-ray structure of ligand (**H_2L**) shows its existence in amido form. All the complexes exhibited a significant inhibitory activity against both Gram-positive and Gram-negative bacteria. Highest antifungal activity was shown by compound (**6**) against *Fusarium solani*. Compound (**3**) displayed highest cytotoxicity among the synthesized compounds with LD_{50} 0.44 μg/mL.

Acknowledgements The authors are thankful to Higher Education Commission of Pakistan for the financial support.

References

Anwer J, Ali S, Shahzadi S, Shahid M, Sharma SK, Qanungo K (2013) Synthesis, characterization, semi-empirical study and biological activities of homobimetallic complexes of tranexamic acid with organotin(IV). J Coord Chem 66:1142–1152. https://doi.org/10.1080/00958972.2013.776678

Armarego WL, Chai CLL (2013) Purification of laboratory chemicals. Butterworth-Heinemann, USA

Atta-ur-Rahman CM, Thomsen WJ (2001) Bioassay techniques for drug development. Harwood Academic Publishers, The Netherlands

Ayers PW, Anderson JS, Bartolotti LJ (2005) Perturbative perspectives on the chemical reaction prediction problem. Int J Quantum Chem 101:520–534. https://doi.org/10.1002/qua.20307

Ayoko GA, Bonire JJ, Abdulkadir SS, Olurinola PF, Ehinmidu JO, Kokot S, Yiasel S (2003) A multicriteria ranking of organotin(IV) compounds with fungicidal properties. Appl Organomet Chem 17:749–758. https://doi.org/10.1002/aoc.520

Becke AD (1988) Density-functional exchange-energy approximation with correct asymptotic behavior. Phys Rev A 38:3098. https://doi.org/10.1103/PhysRevA.38.3098

Beurskens P, Beurskens G, De Gelder R, Garcia-Granda S, Gould R, Israel R, Smits J (1999) The DIRDIF-99 program system. Crystallography Laboratory, University of Nijmegen, Nijmegen

Borba A, Albrecht M, Gómez-Zavaglia A, Suhm MA, Fausto R (2010) Low temperature infrared spectroscopy study of pyrazinamide: from the isolated monomer to the stable low temperature crystalline phase. J Phys Chem A 114:151–161. https://doi.org/10.1021/jp907466h

Bruker S (2006) SAINTPLUS and XPREP. Area Detector Control and Integration Software. Smart Apex Software Reference Manuals. Bruker Analytical X-ray Instruments Inc, Madison

Chaudhary P, Swami M, Sharma D, Singh R (2009) Ecofriendly synthesis, antimicrobial and antispermatogenic activity of triorganotin (IV) complexes with 4′-nitrobenzanilide semicarbazone and 4′-nitrobezanilide thiosemicarbazone. Appl Organomet Chem 23:140–149. https://doi.org/10.1002/aoc.1484

Chermette H (1999) Chemical reactivity indexes in density functional theory. J Comput Chem 20:129–154. https://doi.org/10.1002/(SICI)1096-987X(19990115)20:1<129:AID-JCC13>3.0.CO;2-A

Dennington R, Keith T, Millam JG (2009) GaussView, Ver. 5.0.9 Semichem Inc, Shawnee Mission KS USA

Fani S, Kamalidehghan B, Lo KM, Hashim NM, Chow KM, Ahmadipour F (2015) Synthesis, structural characterization, and anticancer activity of a monobenzyltin compound against MCF-7 breast cancer cells. Drug Des Devel Ther 9:6191–6201. https://doi.org/10.2147/DDDT.S87064

Finney D (1971) Probit analysis, 3rd edn. Cambridge University Press, London

Frisch M et al. (2009) Gaussian 09, revision D. 01. Gaussian, Inc., Wallingford CT

Fukushima K, Dubey SK, Suzuki S (2012) YgiW homologous gene from Pseudomonas aeruginosa 25 W is responsible for tributyltin resistance. J Gen Appl Microbiol 58:283–289. https://doi.org/10.2323/jgam.58.283

Geerlings P, De Proft F (2008) Conceptual DFT: the chemical relevance of higher response functions. PCCP 10:3028–3042. https://doi.org/10.1039/B717671F

Geerlings P, De Proft F, Langenaeker W (2003) Conceptual density functional theory. Chem Rev 103:1793–1874. https://doi.org/10.1021/cr990029p

Gholivand K, EbrahimiValmoozi AA, Gholami A, Dusek M, Eigner V, Abolghasemi S (2016) Synthesis, characterization, crystal structures, QSAR study and antibacterial activities of organotin bisphosphoramidates. J Organomet Chem 806:33–44. https://doi.org/10.1016/j.jorganchem.2015.09.030

Girasolo MA, Attanzio A, Sabatino P, Tesoriere L, Rubino S, Stocco G (2014) Organotin(IV) derivatives with 5,7-disubstituted-1,2,4-triazolo[1,5-a]pyrimidine and their cytotoxic activities: the importance of being conformers. Inorg Chim Acta 423(Part B):168–176. https://doi.org/10.1016/j.ica.2014.07.015

Holeček J, Lyčka A (1986) Dependence of| 1J (119Sn13C)| on the C- Sn- C angle in n-butyltin (IV) compounds. Inorg Chim Acta 118:L15–L16

Hong M, Yin H-D, Cui J-C (2011) Weakly-bridged dimeric diorganotin (IV) compounds derived from pyruvic acid hydrazone Schiff base ligands: synthesis, characterization and crystal structures. Solid State Sci 13:501–507. https://doi.org/10.1016/j.solidstatesciences.2010.11.010

Kohn W, Becke AD, Parr RG (1996) Density functional theory of electronic structure. J Phys Chem 100:12974–12980. https://doi.org/10.1021/jp960669l

Kovala-Demertzi D, Dokorou V, Primikiri A, Vargas R, Silvestru C, Russo U, Demertzis MA (2009) Organotin meclofenamic complexes: synthesis, crystal structures and antiproliferative activity of the first complexes of meclofenamic acid—Novel antituberculosis agents. J Inorg Biochem 103:738–744. https://doi.org/10.1016/j.jinorgbio.2009.01.014

Lee C, Yang W, Parr R (1988) Development of the Colle-Salvetti correlation-energy formula into a functional of the electron density. Phys Rev B: Condens Matter 37(2):785–789

Lockhart TP, Manders WF (1986) Structure determination by NMR spectroscopy. Dependence of| 2J (119Sn, 1H)| on the Me-Sn-Me angle in methyltin(IV) compounds. Inorg Chem 25:892–895. https://doi.org/10.1021/ic00227a002

Meetsma A (2001) PLUTO. Molecular graphics program. University of Groningen, The Netherlands

Muhammad N, Zia-Ur-Rehman Shujah S, Shah A, Ali S, Meetsma A, Hussain Z (2012) Syntheses, structural characteristics, and antimicrobial activities of new organotin (IV) 3-(4-bromophenyl)-2-ethylacrylates. J Coord Chem 65:3766–3775. https://doi.org/10.1080/00958972.2012.718076

Parr R, Yang W (1989) Density functional theory of atoms and molecules. Oxford Univ Press, New York

Parr RG, Yang W (1995) Density-functional theory of the electronic structure of molecules. Annu Rev Phys Chem 46:701–728. https://doi.org/10.1146/annurev.pc.46.100195.003413

Pettinari C, Marchetti F, Pettinari R, Martini D, Drozdov A, Troyanov S (2001) Synthesis and characterisation of tin (IV) and organotin (IV) derivatives 2-{[(2-hydroxyphenyl) imino] methyl} phenol. Inorg Chim Acta 325:103–114. https://doi.org/10.1016/S0020-1693(01)00654-5

Rehman W, Baloch MK, Badshah A (2008) Synthesis, spectral characterization and bio-analysis of some organotin (IV) complexes. Eur J Med Chem 43:2380–2385. https://doi.org/10.1016/j.ejmech.2008.01.019

Roy M, Roy S, Singh KS, Kalita J, Singh SS (2016) Synthesis, characterisation and anti-diabetic activities of triorganotin (IV) azocarboxylates derived from amino benzoic acids and resorcinol: crystal structure and topological study of a 48 membered macrocyclic-tetrameric trimethyltin(IV) complex. Inorg Chim Acta 439:164–172. https://doi.org/10.1016/j.ica.2015.10.012

Sharma S, Meena R, Singh RV, Fahmi N (2016) Synthesis, characterization, antimicrobial, and DNA cleavage evaluation of some organotin(IV) complexes derived from ligands containing the 1H-indole-2,3-dione moiety. Main Group Met Chem 39:31–40. https://doi.org/10.1515/mgmc-2015-0030

Sheldrick G (1997) SHELX-97: Programs for crystal structure analysis Göttingen, Germany

Shpakovsky D et al (2014) Synthesis, antiradical activity and in vitro cytotoxicity of novel organotin complexes based on 2, 6-di-tert-butyl-4-mercaptophenol. Dalton Trans 43:6880–6890. https://doi.org/10.1039/C3DT53469C

Shujah S, Muhammad N, Ali S, Khalid N, Tahir MN (2011) New dimeric and supramolecular organotin (IV) complexes with a tridentate schiff base as potential biocidal agents. J Organomet Chem 696:2772–2781. https://doi.org/10.1016/j.jorganchem.2011.04.010

Shujah S, Muhammad N, Shah A, Ali S, Khalid N, Meetsma A (2013) Bioactive hepta-and penta-coordinated supramolecular diorganotin (IV) Schiff bases. J Organomet Chem 741:59–66. https://doi.org/10.1016/j.jorganchem.2013.05.019

Sirajuddin M, Ali S, McKee V, Zaib S, Iqbal J (2014) Organotin(iv) carboxylate derivatives as a new addition to anticancer and antileishmanial agents: design, physicochemical characterization and interaction with Salmon sperm DNA. RSC Adv 4:57505–57521. https://doi.org/10.1039/C4RA10487K

Spek A (1998) PLATON. Program for the Automated Analysis of Molecular Geometry

Tariq M, Ali S, Muhammad N, Shah NA, Sirajuddin M, Tahir MN, Khalid N, Khan MR (2014) Biological screening, DNA interaction studies, and catalytic activity of organotin (IV) 2-(4-ethylbenzylidene) butanoic acid derivatives: synthesis, spectroscopic characterization, and X-ray structure. J Coord Chem 67:323–340. https://doi.org/10.1080/00958972.2014.884217

Zhang Y-Y, Zhang R-F, Zhang S-L, Cheng S, Li Q-L, Ma C-L (2016) Syntheses, structures and anti-tumor activity of four new organotin(iv) carboxylates based on 2-thienylselenoacetic acid. Dalton Trans 45:8412–8421. https://doi.org/10.1039/C6DT00532B

Zia ur R, Muhammad N, Shuja S, Ali S, Butler IS, Meetsma A, Khan M (2009) New dimeric, trimeric and supramolecular organotin(IV) dithiocarboxylates: synthesis, structural characterization and biocidal activities. Polyhedron 28:3439–3448. https://doi.org/10.1016/j.poly.2009.07.025